Walsh-Hadamard Precoded Circular Filterbank Multicarrier Communications

Quang Duong and Ha H. Nguyen
Department of Electrical and Computer Engineering
University of Saskatchewan, Saskatoon, SK, Canada, S7J 4E3
E-mail: {quang.ddt, ha.nguyen}@usask.ca

***Abstract*—Circular filter bank multicarrier communication (C-FBMC) is an emerging multicarrier communication technique which combines the classical FBMC/OQAM with circular convolution. It has a block based structure and achieves orthogonality among subcarriers. This paper applies Walsh-Hadamard precoding scheme to C-FBMC to exploit the frequency diversity in a multipath channel. The theoretical approximation for the bit error rate (BER) of the resultant scheme, abbreviated WHT-C-FBMC, is derived. Its BER performance is also compared to the performance of precoded GFDM. Results show that the theoretical results match well with simulation results and WHT-C-FBMC is superior than WHT-GFDM.**

I. Introduction

The fifth generation (5G) of cellular networks is coming [1]. One of the main requirements of 5G networks is to increase the data rate about 1000 times the current data rate of 4G networks [2]. To support such a huge rate increase, intensive research on the physical layer – the waveform design has been carried out. Orthogonal frequency division multiplexing (OFDM), which is the dominant technology for 4G networks, can still be a good candidate for 5G networks since it has good qualities such as efficient implementation, single tap equalization for each subcarrier, and being easy to pair with MIMO. However, the high peak-to-average-power ratio (PAPR) and spectral sidelobes of OFDM signals need to be addressed.

Generalized frequency division multiplexing (GFDM) is proposed for the air interface of 5G networks in [3]. In GFDM, the information symbols are organized in an array of subcarriers and subsymbols. The complex symbols on each subcarrier are filtered with a filter that is circularly shifted in time and frequency of a prototype filter. Filtering helps to improve the spectrum localization of GFDM signals. However, it makes subcarrier signals no longer orthogonal, hence resulting in both inter-symbol interference (ISI) and inter-carrier interference (ICI). Nevertheless, efficient detection techniques can eliminate this interference. In particular, for an additive white Gaussian noise (AWGN) channel, a receiver based on the matched filter and iterative interference cancellation [4] can achieve almost the same symbol error rate of an OFDM system. In a frequency selective channel (FSC), [5] proposes a combination of GFDM with the Walsh-Hadamard transform (WHT) to achieve frequency diversity and improve the system performance.

Filter-bank multicarrier (FBMC) modulation is another candidate for 5G networks [6]. The key feature of this technique is to separate the complex data symbols into real and imaginary parts, and introduce a $\pi/2$ offset over consecutive real symbols on adjacent subcarriers and time slots. By this way, the orthogonality of subcarriers can be maintained in the real field with pulse shapes being different from the rectangular window. Recently, [7] and [8] propose the use of cyclic prefix (CP) in FBMC to ease the equalization task at the receiver when operating over a FSC. In a CP-FBMC system, if the CP is directly inserted to the front of the transmitted signal, the overhead can be significantly high due to the linear convolution between input data symbols and the prototype filter in each data block. This is because by using a transmit filter different from the rectangular window, the linear convolution requires that the length of CP accommodates the length of multipath channel plus the length of transmit filter to achieve free interblock interference (IBI) [9]. To achieve free IBI without increasing the length of CP, reference [8] replaces linear convolution used in FBMC with a circular convolution, creating a new scheme called circular FBMC (C-FBMC).

Since C-FBMC is analogous to GFDM, several research works provide comparisons of the two techniques. Reference [10] compares C-FBMC with GFDM in terms of the bit error rate and implementation complexity over an AWGN channel. The authors conclude that GFDM and C-FBMC perform more or less the same for small constellation sizes and when the number of symbols per packet is odd. As the constellation size increases, C-FBMC performs significantly better than GFDM. The authors in [8] provide extensive comparisons of C-FBMC and other candidate waveforms for 5G. The paper also proposes efficient implementations for the transceivers. However, to the best of the authors' knowledge there is no study on precoding techniques for C-FBMC to harvest frequency diversity in FSCs.

This paper applies WHT to C-FBMC to improve its bit error rate (BER) performance over FSCs. In a FSC, the performance of C-FBMC might be severely affected by a few bad subcarriers, which experience deep fade. To address this issue, an unitary precoder is widely used so that the information symbols are distributed on all subcarriers and the information can still be recovered even when the channel severely attenuates a subset of subcarriers. Among many types of precoder, the WHT precoder is adopted in this paper since it has equal-magnitude elements and can be implemented with only additions [9]. The theoretical approximation for the BER

978-1-5090-2291-5/17/$31.00 ©2017 IEEE

of the resultant scheme, WHT-C-FBMC, is derived. Its BER performance is also compared to the performance of precoded GFDM.

The rest of the paper is organized as follows. In Section II, the system model for WHT-C-FBMC is introduced. Performance analysis is presented in Section III. Section IV compares performance of the proposed scheme with that of WHT-GFDM scheme. Section V concludes the paper.

II. System Model

In the proposed WHT-C-FBMC system, the information symbols are processed in blocks, each involving K subcarriers and M time slots. Let $s_{k,m} = s^R_{k,m} + j s^I_{k,m}$ be the complex QAM data symbol associated with the kth subcarrier and mth time slot. To enable offset QAM (OQAM) modulation, the real and imaginary parts of a complex QAM symbol are separated and arranged in a $K \times 2M$ matrix as follows:

$$\begin{aligned}\mathbf{A} &= \begin{bmatrix} a_{0,0} & a_{0,1} & \cdots & a_{0,2M-1} \\ a_{1,0} & a_{1,1} & \cdots & a_{1,2M-1} \\ \vdots & \vdots & \ddots & \vdots \\ a_{K-1,0} & a_{K-1,1} & \cdots & a_{K-1,2M-1} \end{bmatrix} \\ &= \begin{bmatrix} s^R_{0,0} & s^I_{0,0} & \cdots & s^R_{0,M-1} & s^I_{0,M-1} \\ s^R_{0,0} & s^I_{0,0} & \cdots & s^R_{0,M-1} & s^I_{0,M-1} \\ \vdots & \vdots & \ddots & \vdots & \\ s^R_{0,0} & s^I_{0,0} & \cdots & s^R_{0,M-1} & s^I_{0,M-1} \end{bmatrix}. \end{aligned} \tag{1}$$

The block diagram of the WHT-C-FBMC transmitter is illustrated in Fig. 1, where the K data streams inputs are the K rows of matrix $\mathbf{A}$. This structure is basically the polyphase structure presented in [8], except that a WHT precoder is applied to the input.

The WHT is applied for each column of $\mathbf{A}$ as

$$\tilde{\mathbf{a}}_m = \mathbf{W}_K \mathbf{a}_m, \tag{2}$$

where $\mathbf{a}_m$ is the mth column of $\mathbf{A}$, $\mathbf{W}_K$ is a $K \times K$ Walsh-Hadamard matrix and $\tilde{\mathbf{a}}_m$ is the mth precoded column vector.

$$\mathbf{W}_K = \frac{1}{\sqrt{K}} \begin{bmatrix} \mathbf{W}_{K/2} & \mathbf{W}_{K/2} \\ \mathbf{W}_{K/2} & -\mathbf{W}_{K/2} \end{bmatrix}, \ \mathbf{W}_2 = \frac{1}{\sqrt{2}} \begin{bmatrix} 1 & 1 \\ 1 & -1 \end{bmatrix}. \tag{3}$$

In an OQAM system, the phase offsets are introduced to the real and imaginary components of QAM symbols on different subcarriers as follows:

$$\mathbf{b}_m = \mathbf{J}_m \tilde{\mathbf{a}}_m \tag{4}$$

where $\mathbf{J}_m = \mathrm{diag}([j^m, j^{m+1}, \ldots, j^{m+K-1}])$. Then, the WHT-C-FBMC transmitted signal is then given as [7]

$$x[n] = \sum_{k=0}^{K-1} \sum_{m=0}^{2M-1} j^{k+m} \tilde{a}_{k,m} g[(n - mK/2)_{KM}] \mathrm{e}^{j2\pi kn/K}, \tag{5}$$

where $n = 0, 1, \ldots, KM-1$, $\tilde{a}_{k,m}$ is the kth element of $\tilde{\mathbf{a}}_m$, $g[n]$ is the impulse response of a prototype filter, which has KM coefficients, and $g[(n-z)_w]$ denotes cyclically shifting $g[n]$ by z positions with period w.

The polyphase structure [8] for the implementation of (5) as shown in Fig. 1 is the most efficient method and can be described clearly in matrix form. Let $\mathbf{x} = [x[0], x[1], \ldots, x[KM-1]]^\top$, and $\mathbf{g} = [g[0], g[1], \ldots, g[KM-1]]^\top$ be the transmitted vector and vector of filter coefficients, respectively. Then the matrix form representation of (5) is

$$\mathbf{x} = \sum_{m=0}^{2M-1} \mathbf{G}_m \mathbf{R} \mathbf{F}_K^H \mathbf{b}_m, \tag{6}$$

where $\mathbf{F}_K$ is the K-point FFT matrix, $\mathbf{R} = [\mathbf{I}_K, \ldots, \mathbf{I}_K]^\top$, $\mathbf{G}_m = \mathrm{diag}(\mathbf{\Phi}_m \mathbf{g}) = \mathrm{diag}([g_{0,m}, g_{1,m}, \ldots, g_{KM-1,m}])$, and $\mathbf{\Phi}_m$ is a $KM \times KM$ circulant matrix whose first column has only one non zero value, which is the $(mK/2)$th element with value 1. In this structure, $\mathbf{b}_m$ is first transformed into the time domain by multiplying it with an inverse FFT matrix, $\mathbf{F}_K^H$. Upsampling is performed by repeating the $K \times 1$ transformed vector M times with the $KM \times K$ matrix $\mathbf{R}$. The resulted vector is pulse-shaped by point-wise multiplication with the circularly shifted version of the prototype filter, which is $\mathbf{\Phi}_m \mathbf{g}$. Then the transmitted signal is obtained by summing all pulse-shaped subsymbol vectors. Substituting (2) and (4) into (6), the transmitted signal of WHT-C-FBMC can be expressed as

$$\mathbf{x} = \sum_{m=0}^{2M-1} \mathbf{G}_m \mathbf{R} \mathbf{F}_K^H \mathbf{J}_m \mathbf{W}_K \mathbf{a}_m, \tag{7}$$

In a multipath channel, C-FBMC uses a cyclic prefix (CP) of length L to achieve free inter-block interference (IBI). Let $\mathbf{h} = [h[0], h[1], \cdots, h[V-1]]^\top$ ($V \ll KM$) be the vector of an V-taps channel impulse response. As long as $V - 1 \leq L$, free IBI is guaranteed at the receiver. In that case, the received signal after removing CP can be written as

$$\mathbf{y} = \mathbf{H}\mathbf{x} + \mathbf{n}, \tag{8}$$

where $\mathbf{H}$ is a $KM \times KM$ circulant matrix whose first column is $\mathbf{h}$ appended with $KM - V$ zeros, and $\mathbf{n}$ is a vector of additive while Gaussian noise (AWGN) samples.

An approach to demodulate data is described in Fig. 1 [8]. First, an equalizer $\mathbf{S}$ is applied to the received signal $\mathbf{y}$ to remove the effect of multipath interference. Then, the equalized vector is processed in dual to (7). The equalized output that can be used to detect the data symbol for the mth time slot is given by

$$\hat{\mathbf{a}}_m = \mathbf{W}_K^H \Re\{\mathbf{J}_m^H \mathbf{F}_K \mathbf{R}^\top \mathbf{G}_m \mathbf{S} \mathbf{y}\}. \tag{9}$$

In an ideal channel where $\mathbf{y} = \mathbf{x}$, the equalized signal is

$$\hat{\mathbf{a}}_m = \mathbf{W}_K^H \mathcal{R} \left\{ \mathbf{J}_m^H \mathbf{F}_K \mathbf{R}^\top \mathbf{G}_m \sum_{m=0}^{2M-1} \mathbf{G}_m \mathbf{R} \mathbf{F}_K^H \mathbf{J}_m \mathbf{W}_K \mathbf{a}_m \right\}. \tag{10}$$

Since the elements of $\mathbf{a}_m$ and $\mathbf{W}_K$ are real, (10) is rewritten as

$$\hat{\mathbf{a}}_m = \mathbf{W}_K^H \mathcal{R} \left\{ \mathbf{J}_m^H \mathbf{F}_K \mathbf{R}^\top \mathbf{G}_m \sum_{m=0}^{2M-1} \mathbf{G}_m \mathbf{R} \mathbf{F}_K^H \mathbf{J}_m \right\} \mathbf{W}_K \mathbf{a}_m \tag{11}$$

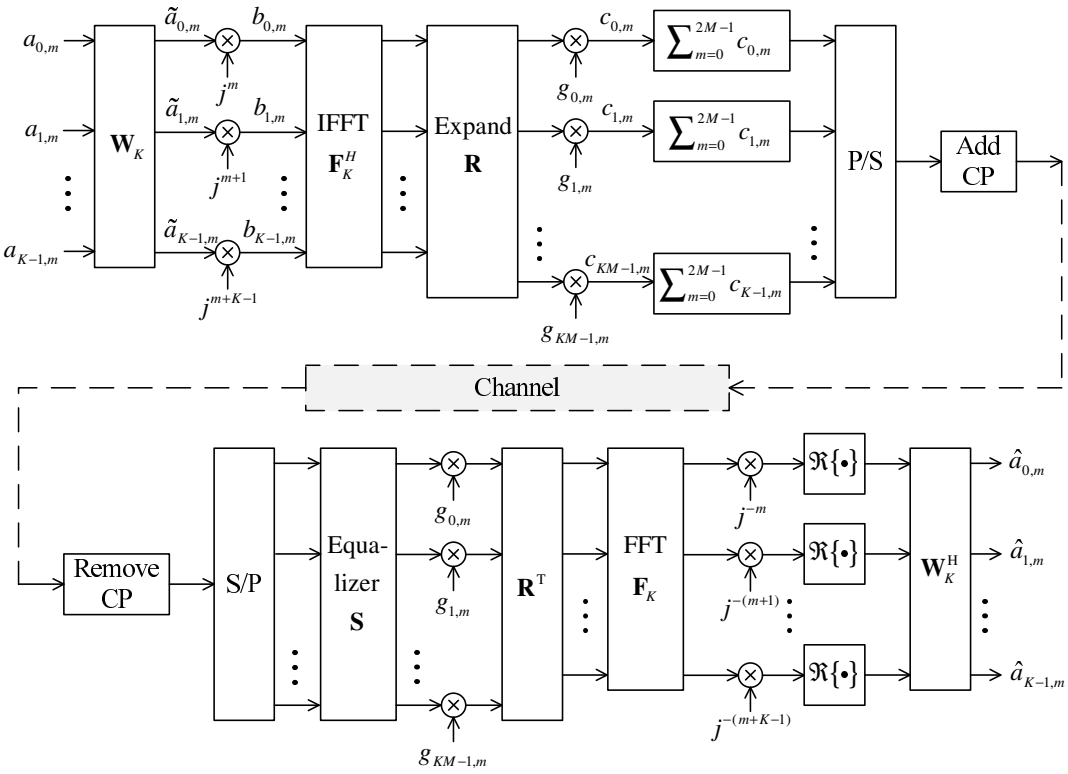

Fig. 1: Equivalent complex baseband WHT-C-FBMC system.

Because $\mathbf{W}_K^H\mathbf{W}_K = \mathbf{I}$, perfect reconstruction is achieved, i.e., $\hat{\mathbf{a}}_m = \mathbf{a}_m$ if the following condition is satisfied:

$$\mathcal{R}\left\{\mathbf{J}_m^H\mathbf{F}_K\mathbf{R}^\top\mathbf{G}_m\mathbf{G}_{m'}\mathbf{R}\mathbf{F}_K^H\mathbf{J}_{m'}\right\} = \begin{cases} \mathbf{I}, & \text{if} \quad m = m' \\ \mathbf{0}, & \text{if} \quad m \neq m' \end{cases}, \tag{12}$$

where $\mathbf{0}$ is the $K \times K$ zero matrix. To guarantee perfect reconstruction, in FBMC, the combined response of the transmit filter and received filter must be a Nyquist pulse [11]. A standard square-root raise cosine (SRRC) filter fulfills such a condition and is widely employed for FBMC. More recently, [12] proves that a pulse satisfying the orthogonality condition for FBMC also satisfies the orthogonality condition for C-FBMC. This paper simply employs a SRRC filter of length KM where the coefficients are real and symmetric such that $g[n] = g[KM - n]$.

III. Performance Analysis of WHT-C-FBMC

Consider the zero-forcing equalizer, i.e., $\mathbf{S} = \mathbf{H}^{-1}$. Then (9) becomes

$$\hat{\mathbf{a}}_m = \mathbf{W}_K^H\mathcal{R}\left\{\mathbf{J}_m^H\mathbf{F}_K\mathbf{R}^\top\mathbf{G}_m\mathbf{H}^{-1}\left[\mathbf{H}\mathbf{x} + \mathbf{n}\right]\right\}. \tag{13}$$

As long as (12) is fulfilled with a well designed prototype filter, (13) is rewritten as

$$\hat{\mathbf{a}}_m = \mathbf{a}_m + \hat{\mathbf{n}}_m, \tag{14}$$

where the filtered noise vector $\hat{\mathbf{n}}_m$ is

$$\hat{\mathbf{n}}_m = \mathbf{W}_K^H\mathcal{R}\left\{\mathbf{Q}_m\mathbf{n}\right\} \tag{15}$$

and

$$\mathbf{Q}_m = \mathbf{J}_m^H\mathbf{F}_K\mathbf{R}^\top\mathbf{G}_m\mathbf{H}^{-1}. \tag{16}$$

Since $\mathbf{n}$ is a circularly symmetric Gaussian random vector which with correlation matrix $N_0\mathbf{I}$, the correlation of $\hat{\mathbf{n}}_m$ is

$$\mathbf{E}\{\hat{\mathbf{n}}_m\hat{\mathbf{n}}_m^H\} = \frac{N_0}{2}\mathbf{W}_K^H\mathcal{R}\left\{\mathbf{Q}_m\mathbf{Q}_m^H\right\}\mathbf{W}_K. \tag{17}$$

The term $\mathcal{R}\left\{\mathbf{Q}_m\mathbf{Q}_m^H\right\}$ is a diagonal matrix whose diagonal elements are

$$\left[\mathcal{R}\left\{\mathbf{Q}_m\mathbf{Q}_m^H\right\}\right]_{k,k} = \frac{1}{KM}\sum_{n=0}^{KM-1}\frac{|\sum_{i=0}^{KM-1} g_{i,m}\mathrm{e}^{-j\phi_{i,n,k,m}}|^2}{|H_n|^2}, \tag{18}$$

where

$$\phi_{i,n,k,m} = \left[-\frac{\pi}{2}(k+m) - \frac{2\pi}{K}(i \mod K) + \frac{2\pi}{KM}ni\right], \tag{19}$$

and H_k is the kth component of the channel frequency response of $\mathbf{h}$, i.e., $H_k = \sum_{n=0}^{KM-1} h_n\mathrm{e}^{-j2\pi kn/(KM-1)}$. The proof of (18) is provided in the Appendix. It then follows that the diagonal elements of the correlation matrix in (17) are

$$\left[\mathbf{E}\{\hat{\mathbf{n}}_m\hat{\mathbf{n}}_m^H\}\right]_{k,k} = \frac{N_0}{2}\sum_{l=0}^{K-1}|w_{k,l}|^2\left[\mathcal{R}\left\{\mathbf{Q}_m\mathbf{Q}_m^H\right\}\right]_{l,l}. \tag{20}$$

The Walsh-Hadamard matrix has the property that $|w_{k,l}| = \frac{1}{\sqrt{K}}$ for all k, l. Therefore, the noise correlation matrix has identical diagonal elements, which are

$$\left[\mathbf{E}\{\hat{\mathbf{n}}_m\hat{\mathbf{n}}_m^H\}\right]_{k,k} = \frac{N_0}{2K^2M}\sum_{l=0}^{K-1}\sum_{n=0}^{KM-1}\frac{|\sum_{i=0}^{KM-1} g_{i,m}\mathrm{e}^{-j\phi_{i,n,l,m}}|^2}{|H_n|^2}. \quad (21)$$

The BER of a WHT-C-FBMC system can be obtained based on the signal-to-noise ratio (SNR) associated with the equivalent input/output expression in (14). Let $E_s = \mathbf{E}\left\{|s_{k,m}|^2\right\}$ be the average transmitted energy of the QAM symbols. Furthermore, assume that the real and imaginary components of the QAM signal have equal energy, i.e., $\mathbf{E}\left\{|a_{k,m}|^2\right\} = E_s/2$. Then the SNR corresponding to the detection of $a_{k,m}$ is

$$\beta_{k,m} = \frac{E_s/2}{[\mathbf{E}\{\hat{\mathbf{n}}_m\hat{\mathbf{n}}_m^H\}]_{k,k}} = \frac{\gamma_s K^2 M}{\sum_{l=0}^{K-1}\sum_{n=0}^{KM-1}\frac{|\sum_{i=0}^{KM-1} g_{i,m}\mathrm{e}^{-j\phi_{i,n,l,m}}|^2}{|H_n|^2}}, \quad (22)$$

where $\gamma_s = E_s/N_0$. Equation (22) implies that $\beta_{k,m}$ does not depend on k since the operation of Wash-Hadamard matrix averages the SNR over all subcarriers. Then, one can write

$$\beta_{k,m} = \beta_m = \frac{\gamma_s}{\alpha_m} \quad \text{for all } k, \quad (23)$$

where

$$\alpha_m = \frac{1}{K^2M}\sum_{l=0}^{K-1}\sum_{n=0}^{KM-1}\frac{|\sum_{i=0}^{KM-1} g_i\mathrm{e}^{-j\phi_{i,n,l,m}}|^2}{|H_n|^2}. \quad (24)$$

The BER with 2^μ-QAM constellation with Gray coding is well approximated as

$$P_{\mathrm{WHT-CFBMC}} = \frac{4}{\mu M}\left(1-\frac{1}{2^{\mu/2}}\right)\sum_{m=0}^{M-1} Q\left(\sqrt{\frac{3\mu\gamma_b}{\alpha_m(2^\mu-1)}}\right), \quad (25)$$

where $\gamma_b = \frac{E_b}{N_0}$ and $E_b = E_s/\mu$ is the energy per bit. It is pointed out that α solely depends on the coefficients of the prototype filter, and the channel coefficients.

IV. Simulation Results

Fig. 2 and Fig. 3 present the BER performance of GFDM/WHT-GFDM and C-FBMC/WHT-C-FBMC under two different FSCs, each for two constellations of 4-QAM and 64-QAM. The delay profiles of the two channels are provided in Table II. GFDM and CFBMC signals are transmitted block by block, where one block has KM symbols. In the simulation, the duration of a time slot (subsymbol) is $T = 256\ \mu s$. A block of KM symbols is transmitted over the duration of MT seconds, leading to the sampling period (duration of one symbol) of $T_s = MT/KM = T/K = 4\ \mu s$. An L-paths channel can be modelled by a V-tap discrete filter as [13]

$$h[v] = \sum_{l=0}^{L-1}|q_l|\mathrm{e}^{j\phi_l}\ \mathrm{sinc}\left[v-\frac{\tau_l}{T_s}\right] \quad v = 0,1,\ldots,V-1, \quad (26)$$

TABLE I: Simulation parameters.

Parameters	Value
Number of subcarriers (K)	64
Number of subsymbols (M)	32
Prototype filter	SRRC
Roll-off	0.5
Modulation	4-QAM, 64-QAM
FSC	$h[n] \sim \mathcal{CN}(0, 10^{-\frac{n}{V-1}})$

TABLE II: Delay profile used in simulation

Ch. A	Gain (dB)	0	-8	-14	-	-	-	-
	Delay (μs)	0	4.57	9.14	-	-	-	-
Ch. B	Gain (dB)	0	-10	-12	-13	-16	-20	-22
	Delay (μs)	0	2.85	4.57	6.28	9.71	15.43	20

where τ_l, and $|q_l|\mathrm{e}^{j\phi_l}$ is the delay, and complex gain of the lth path, respectively. In the simulation, $|q_l|$ is computed based on the specified dB gain of each path, and ϕ_l is generated randomly in the range $[0, 2\pi]$. The value of V is chosen such that $|h[v]|$ is small when v is greater than V.

Fig. 2 shows that WHT-C-FBMC performs 2.5 dB better than WHT-GFDM at the BER level of 10^{-4} even with a large constellation such as 64-QAM. Since WHT-GFDM is based on GFDM, which is a non-orthogonal system, the interference between subsymbols and subcarriers is intensified in a FSC. That makes the BER performances of WHT-GFDM worse than that of WHT-C-FBMC, which is an orthogonal system. WHT-GFDM and WHT-C-FBMC offer even a larger performance gain under Channel B. Specifically, WHT-GFDM is 5 dB better than the non-precoding scheme, while WHT-C-FBMC achieves 7.5 dB SNR gain at BER $= 10^{-4}$.

Fig. 4 shows that (25) can be used to accurately estimate the BER of WHT-C-FBMC over a FSC. In both channels, with 4-QAM modulation, the theoretical result matches perfectly with that of the simulation result for any SNR value. With 64-QAM modulation, the theoretical approximation is very accurate at SNR larger than 7.5 dB.

V. Conclusion

To enhance the BER performance of C-FBMC in a FSC, this paper studies a precoded version of C-FBMC, called WHT-C-FBMC, which uses the unitary Walsh-Hadamard precoding matrix. WHT-C-FBMC exploits the frequency diversity by averaging the SNR output over all subcarriers. A theoretical approximation for the BER of WHT-C-FBMC has also been provided, which depends on the filter coefficients and channel gains. Results show that WHT-C-FBMC performs significantly better than WHT-GFDM in FSCs.

Appendix

From (16), $\mathcal{R}\left\{\mathbf{Q}_m\mathbf{Q}_m^H\right\}$ is given as

$$\mathcal{R}\left\{\mathbf{Q}_m\mathbf{Q}_m^H\right\} = \mathcal{R}\left\{\mathbf{J}_m^H\mathbf{F}_K\mathbf{R}^\top\mathbf{G}_m\mathbf{H}^{-1}(\mathbf{H}^{-1})^H\mathbf{G}_m\mathbf{R}\mathbf{F}_K^H\mathbf{J}_m\right\} \quad (27)$$

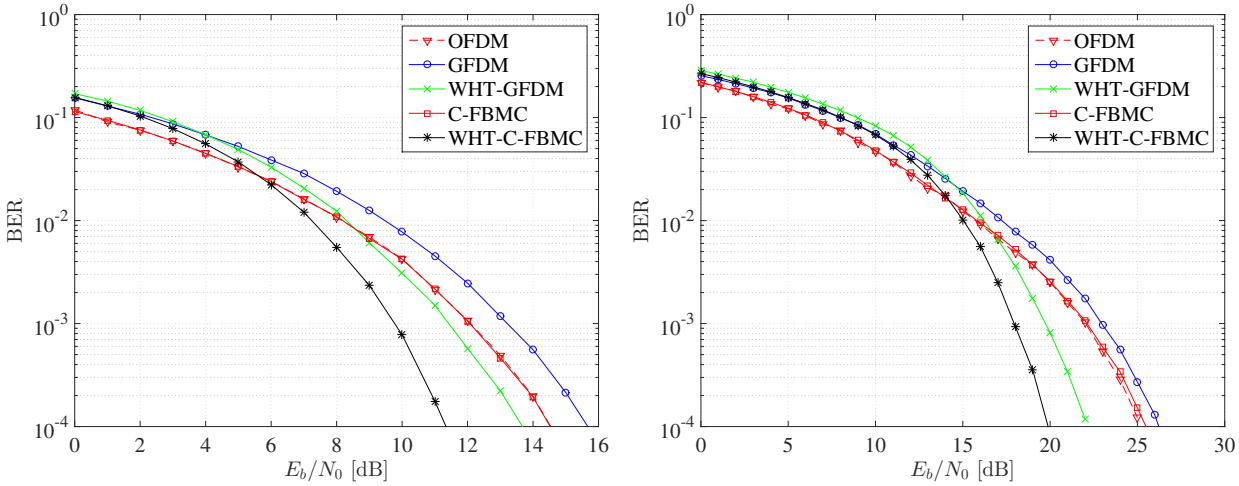

(a) 4-QAM (b) 64-QAM

Fig. 2: WHT-C-FBMC and WHT-GFDM BER performance in FSC Channel A.

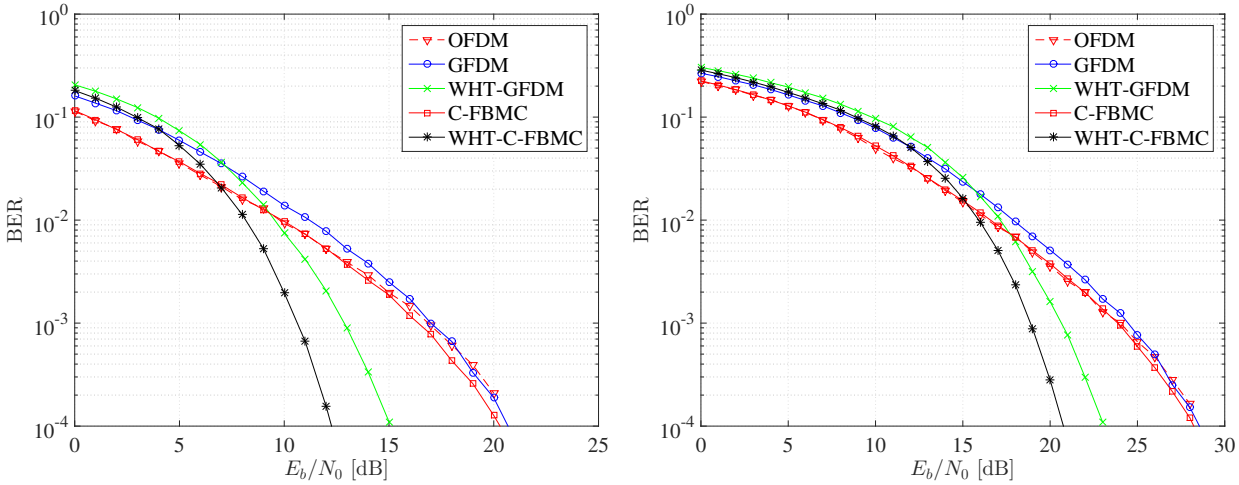

(a) 4-QAM (b) 64-QAM

Fig. 3: WHT-C-FBMC and WHT-GFDM BER performance in FSC Channel B.

Recall that $\mathbf{H}$ is a $KM \times KM$ circulant matrix. Thus, one has $\mathbf{H}^{-1}(\mathbf{H}^{-1})^H = \frac{1}{KM}\mathbf{F}_{KM}^H \mathbf{\Lambda} \mathbf{F}_{KM}$, where $\mathbf{\Lambda} = \mathrm{diag}(|H_0|^{-2}, |H_1|^{-2}, \ldots, |H_{KM-1}|^{-2})$. Rewrite (27) as

$$\mathcal{R}\left\{\mathbf{Q}_m \mathbf{Q}_m^H\right\} = \frac{1}{KM}\mathcal{R}\left\{\mathbf{T}_m \mathbf{\Lambda} \mathbf{T}_m^H\right\} \tag{28}$$

where

$$\mathbf{T}_m = \mathbf{Y}_m \mathbf{F}_{KM}^H, \quad \mathbf{Y}_m = \mathbf{J}_m^H \mathbf{F}_K \mathbf{R}^\top \mathbf{G}_m. \tag{29}$$

The (k,n) elements of $\mathbf{T}_m$ are

$$t_{k,n} = \sum_{i=0}^{KM-1} y_{k,i} \mathrm{e}^{j\frac{2\pi}{KM}ni}, \tag{30}$$

where

$$y_{k,i} = (-j)^{k+m} g_{i,m} \mathrm{e}^{-j\frac{2\pi}{K}k(i \mod K)}. \tag{31}$$

Thus, the elements of $\mathcal{R}\left\{\mathbf{Q}_m \mathbf{Q}_m^H\right\}$ are

$$\left[\mathcal{R}\left\{\mathbf{Q}_m \mathbf{Q}_m^H\right\}\right]_{k,k'} = \frac{1}{KM} \frac{\sum_{n=0}^{KM-1} \mathcal{R}\left\{t_{k,n}(t_{k',n})^*\right\}}{|H_n|^2} \tag{32}$$

For $k = k'$, it is easy to see that using (30) and (31) leads to the expression of $\left[\mathcal{R}\left\{\mathbf{Q}_m \mathbf{Q}_m^H\right\}\right]_{k,k}$ in (18).

For $k \neq k'$, one has

$$\mathcal{R}\left\{t_{k,n}(t_{k',n})^*\right\} = \mathcal{R}\left\{\sum_{i=0}^{KM-1} y_{k,i} \mathrm{e}^{j\frac{2\pi}{KM}ni} \sum_{i'=0}^{KM-1} (y_{k',i'})^* \mathrm{e}^{-j\frac{2\pi}{KM}ni'}\right\}$$

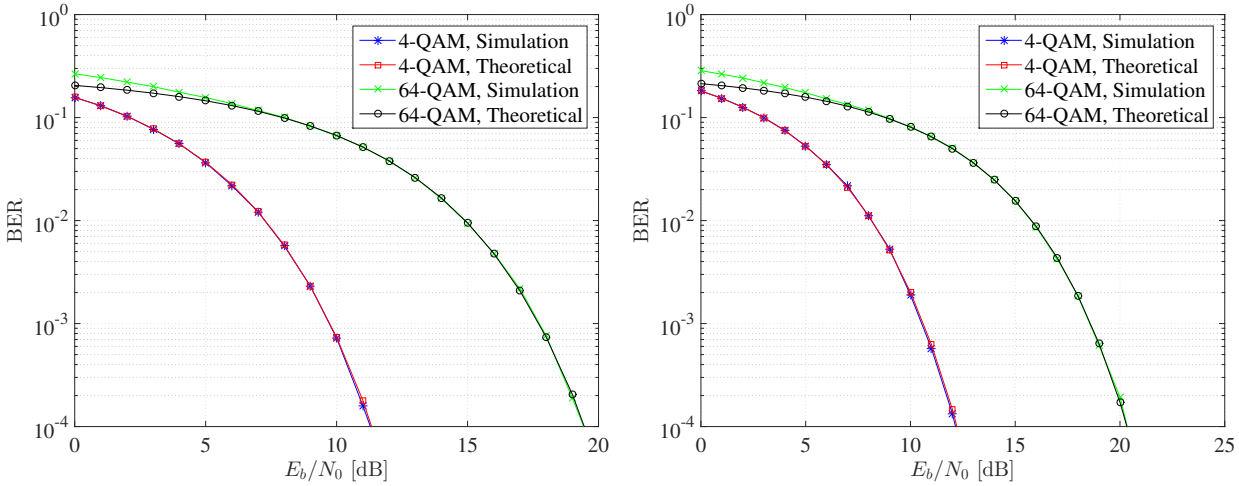

(a) Channel A (b) Channel B

Fig. 4: Simulation versus theoretical results of WHT-CFBMC system.

$$= \mathcal{R}\left\{\sum_{i=0}^{KM-1} y_{k,i}(y_{k',i})^*\right\} + \mathcal{R}\left\{\sum_{i=0}^{KM-1} y_{k,i}\mathrm{e}^{j\frac{2\pi}{KM}ni}\sum_{\substack{i'=0\\ i'\neq i}}^{KM-1} y_{k',i'}\mathrm{e}^{-j\frac{2\pi}{KM}ni'}\right\} \quad (33)$$

From (12), and (31) it can be verified that $\mathcal{R}\left\{\sum_{i=0}^{KM-1} y_{k,i}(y_{k',i})^*\right\} = 0$. In addition, from (31) and the fact that $g_{KM-i,m} = g_{i,m}$ for $i < \frac{KM}{2}$, one has

$$\begin{aligned} y_{k,KM-i} &= (-j)^{k+m} g_{KM-i,m}\mathrm{e}^{-j\frac{2\pi}{K}k(KM-i \mod K)} \\ &= (-j)^{k+m} g_{i,m}\mathrm{e}^{j\frac{2\pi}{K}k(i \mod K)}. \end{aligned} \quad (34)$$

Using (31), and (34), one can verify that

$$\begin{aligned} \mathcal{R}\{y_{k,i}(y_{k',i'})^*\} &= -\mathcal{R}\{y_{k,KM-i}(y^m_{k',KM-i'})^*\} \\ \mathcal{I}\{y_{k,i}(y_{k',i'})^*\} &= \mathcal{I}\{y_{k,KM-i}(y^m_{k',KM-i'})^*\}. \end{aligned} \quad (35)$$

Thus, (33) can be rewritten as

$$\begin{aligned} &\mathcal{R}\{t_{k,n}(t_{k',n})^*\} \\ &= \sum_{i=0}^{KM/2-1} \mathcal{R}\Big\{\Big[y_{k,i}(y_{k',i'})^*\mathrm{e}^{j\frac{2\pi}{KM}n(i-i')} \\ &\quad + y_{k,KM-i}(y^m_{k',KM-i'})^*\mathrm{e}^{-j\frac{2\pi}{KM}n(i-i')}\Big]\Big\} \\ &= \sum_{i=0}^{KM/2-1} \Big[\mathcal{R}\{y_{k,i}(y_{k',i'})^*\}\cos\frac{2\pi}{KM}n(i-i') \\ &\quad - \mathcal{I}\{y_{k,i}(y_{k',i'})^*\}\sin\frac{2\pi}{KM}n(i-i') \\ &\quad + \mathcal{R}\{y_{k,KM-i}(y_{k',KM-i'})^*\}\cos\frac{2\pi}{KM}n(i-i') \\ &\quad + \mathcal{I}\{y_{k,KM-i}(y_{k',KM-i'})^*\}\sin\frac{2\pi}{KM}n(i-i')\Big] \\ &= 0. \end{aligned} \quad (36)$$

REFERENCES

[1] F. Boccardi, R. W. Heath, A. Lozano, T. L. Marzetta, and P. Popovski, "Five disruptive technology directions for 5G," *IEEE Communications Magazine*, vol. 52, pp. 74–80, February 2014.

[2] J. G. Andrews, S. Buzzi, W. Choi, S. V. Hanly, A. Lozano, A. C. K. Soong, and J. C. Zhang, "What will 5G be?," *IEEE Journal on Selected Areas in Communications*, vol. 32, pp. 1065–1082, June 2014.

[3] N. Michailow, M. Matthe, I. S. Gaspar, A. N. Caldevilla, L. L. Mendes, A. Festag, and G. Fettweis, "Generalized frequency division multiplexing for 5th generation cellular networks (invited paper)," *IEEE Transactions on Communications*, vol. 62, pp. 3045–3061, Sept. 2014.

[4] R. Datta, N. Michailow, M. Lentmaier, and G. Fettweis, "GFDM interference cancellation for flexible cognitive radio phy design," in *Proc. IEEE Vehicular Technology Conference*, 2012.

[5] N. Michailow, L. Mendes, M. Matthé, I. Gaspar, A. Festag, and G. Fettweis, "Robust WHT-GFDM for the next generation of wireless networks," *IEEE Communications Letters*, vol. 19, pp. 106–109, Jan. 2015.

[6] B. Farhang-Boroujeny, "OFDM versus filter bank multicarrier," *IEEE Signal Processing Magazine*, vol. 28, pp. 92–112, 2011.

[7] X. Gao, W. Wang, X. G. Xia, E. K. S. Au, and X. You, "Cyclic prefixed OQAM-OFDM and its application to single-carrier FDMA," *IEEE Transactions on Communications*, vol. 59, pp. 1467–1480, May 2011.

[8] H. Lin and P. Siohan, "Multi-carrier modulation analysis and WCP-COQAM proposal," *EURASIP Journal on Advances in Signal Processing*, vol. 2014:79, 19 pages, 2014.

[9] Y.-P. Lin, S.-M. Phong, and P. P. Vaidyanathan, *Filter Bank Transceivers for OFDM and DMT Systems*. Cambridge University Press, 2010.

[10] A. Rezazadeh Reyhani, A. Farhang, and B. Farhang-Boroujeny, "Circularly pulse-shaped waveforms for 5G: Options and comparisons," in *IEEE Global Communications Conference (GLOBECOM)*, pp. 1–7, Dec. 2015.

[11] B. Farhang-Boroujeny and C. H. (George) Yuen, "Cosine modulated and offset QAM filter bank multicarrier techniques: A continuous-time prospect," *EURASIP Journal on Advances in Signal Processing*, vol. 2010, pp. 1–17, 2010.

[12] A. B. Üçüncü and A. Ö. Yilmaz, "Pulse shaping methods for OQAM/OFDM and WCP-COQAM," *http://arxiv.org/abs/1509.00977*, 2015.

[13] D. Tse and P. Viswanath, *Fundamentals of Wireless Communication*. Cambridge University Press, 2005.